Enhanced Blocking Frequencies in Very-high Resolution Idealized Climate Model Simulations

P. De Luca[1,2], B. Jiménez-Esteve[3], L. Degenhardt[2], S. Schemm[4], and S. Pfahl[2]

[1]Barcelona Supercomputing Center (BSC), Barcelona, Spain

[2]Institute of Meteorology - Freie Universität Berlin, Berlin, Germany

[3]Instituto de Geociencias (IGEO), Consejo Superior de Investigaciones Científicas–Universidad Complutense de Madrid (CSIC–UCM), Madrid, Spain

[4]Institute for Atmospheric and Climate Science - ETH Zürich, Zürich, Switzerland

Corresponding author: Paolo De Luca (paolo.deluca@bsc.es)

Key Points:

- Blocking frequency increases downstream and poleward of sea-surface temperature front with convection permitting atmospheric resolution
- The specific region of increased blocking depends on the blocking index
- Changes in diabatic heating and Rossby wave breaking play a fundamental role for the blocking enhancement

Keywords: very-high resolution; climate modeling; ICON; idealized; blocking; wave breaking

Abstract

Atmospheric blocking is a key dynamical phenomenon in the mid- and high latitudes, able to drive day-to-day weather changes and meteorological extremes such as heatwaves, droughts and cold waves. Current global circulation models struggle to fully capture observed blocking frequencies, likely because of their coarse horizontal resolution. Here we use convection permitting, nested idealized model simulations for quantifying changes in blocking frequency and Rossby wave breaking compared to a coarser resolution reference. We find an increase in blocking frequency poleward and downstream of the area with increased resolution, while the exact regions depend on the blocking index. These changes are probably due to a more accurate representation of small-scale processes such as diabatic heating, which affect Rossby wave breaking and blocking formation downstream. Our results thus suggest an improved representation of blocking in the next generation of high-resolution global climate models.

Plain Language Summary

Atmospheric blocking is a persistent weather pattern associated with high-pressure anomalies that is able to drive meteorological extremes such as heatwaves and drought in summer, and cold waves in winter. Having blocking well represented in state-of-the-art climate models is of paramount importance, however these models fail in simulating the frequency of blocking events, likely because their grid resolution is not high enough for resolving small scale physical processes important for the development of blocking episodes. Here we use very-high resolution model simulations for quantifying blocking frequencies and the mechanisms driving these episodes. Our simulations are idealised, in the sense that they do not fully represent the Earth's system but allow us to focus on key physical mechanisms driving the blocking events. Our results show that using a very-high resolution enhances blocking frequencies when compared to a lower resolution grid. The findings point toward the importance that unresolved physical processes play in generating blocking events that can only be simulated at very-high resolution and can be of importance for the next generation of climate models.

1. Introduction

Atmospheric blocking can be considered one of the major features of the mid-latitude circulation that occurs during an anomalous and persistent meandering of the jet stream (Lupo, 2021; Nakamura & Huang, 2018; Woollings et al., 2018). Blocking is defined as a persistent weather pattern, characterized by anticyclonic circulation, high surface pressure and blocked westerlies. Changes in surface temperature, precipitation and wind patterns associated with blocking in turn can evolve into severe weather extremes such as heatwaves and droughts in summer as well as cold waves and low air quality during winter (e.g. Cai et al., 2020; Kautz et al., 2022; Matsueda,

2011; Pfahl & Wernli, 2012). Thus, it is of paramount importance to accurately represent blocking in state-of-the-art coupled climate models to be able to anticipate future changes in the associated extremes events under anthropogenic climate change.

Atmospheric blocking is currently underrepresented in coupled climate models (Davini & D'Andrea, 2020; Pithan et al., 2016; Schiemann et al., 2020; Woollings et al., 2018). Such large biases in the representation of blocking eventually lead to large uncertainties in its future climate projections and, therefore, in representing dynamic mechanisms driving extreme weather phenomena (e.g. heatwaves and droughts). The causes of the underestimation of blocking in climate models are manifold. For example, Pithan et al. (2016) show that a better representation of orographic drag can improve the simulation of European blocking. On the other hand, Scaife et al. (2010) argue that blocking underestimation in climate models relates to the models' climatological mean state bias. They suggest that correcting these mean-state biases improves the representation of blocking and this is in agreement with Narinesingh et al. (2020), who demonstrate, using aquaplanet simulations with idealized orographic forcing, that the mean state highly impacts the blocking frequency climatology.

Another reason for the underestimation of blocking in the latest generation of global climate models, or the Coupled Model Intercomparison Project Phase 6 (CMIP6) models (Eyring et al., 2016), is the horizontal model resolution (Schiemann et al., 2020). Studies show that, to simulate atmospheric blocking, a high horizontal resolution is necessary to capture smaller-scale processes such as eddy vorticity fluxes (e.g. Yamazaki & Itoh, 2013) and diabatic heating in clouds (Pfahl et al., 2015), which in turn sustain blocking events. Schiemann et al. (2020) compare blocking frequency and persistence between CMIP6 and CMIP5 (Taylor et al., 2012) models, and also use HighResMIP simulations (Haarsma et al., 2016) to quantify the effect of horizontal resolution. They find that CMIP6 models better simulate blocking frequency and persistence compared to CMIP5 and that an increase in horizontal resolution in HighResMIP simulations enhances blocking frequency but not persistence in the northern mid-latitudes (Schiemann et al., 2020). Matsueda et al. (2009) investigated future changes in blocking using different horizontal grid spacing, from

20 km to 180 km, in atmospheric global circulation models, and they state that the highest horizontal resolution (i.e. 20 km) is required for properly simulating Euro-Atlantic blocking events. In their follow-up study (Matsueda et al., 2010), where they assess future changes in summer and wintertime blocking over Australia-New Zealand and in the Andes, they also show similar conclusions. In addition, Athanasiadis et al. (2022) demonstrate how climate models' sea-surface temperature cold biases in the central North Atlantic can be improved by deploying an increased horizontal resolution in the ocean. They also show that such bias improvement leads to changes in baroclinicity and diabatic heating, eventually enhancing European blocking events. Scaife et al. (2011) also show that an improvement of the cold North Atlantic oceanic bias, obtained with a higher resolution, leads to improved Atlantic winter blocking frequencies. Despite this importance of horizontal resolution, so far and to our knowledge, there is a lack of a study investigating the representation of blocking and its underlying mechanisms in climate model simulations with km-scale horizontal resolution that allows for an explicit representation of convective processes.

Diabatic heating in ascending air masses plays an important role for blocking formation and maintenance downstream (Hermoso et al., 2024; Pfahl et al., 2015; Steinfeld et al., 2020; Steinfeld & Pfahl, 2019). The ascending air is typically associated with the warm conveyor belt (WCB) of extratropical cyclones, which subsequently forms a negative potential vorticity (PV) anomaly in its outflow region, reinforcing anticyclonic circulation anomalies at upper levels in a developing ridge. Preferred regions for such WCBs are the SST fronts over the western North Atlantic and North Pacific, where many extratropical cyclones develop (Madonna et al., 2014). The formation of a blocking event is thus intrinsically linked to the baroclinic instability and cyclogenesis of extratropical cyclones along the SST-front over the western boundary currents (Steinfeld & Pfahl, 2019; Yamamoto et al., 2021). Here, we hypothesize that an increase in horizontal resolution in this area of SST-front increases diabatic processes linked to cyclone formation and thus increases the WCB outflow that enhances ridge building, anticyclonic flow and eventually blocking formation.

To explore this hypothesis, we build on previous work addressing the impact of horizontal resolution on the simulation of blocking frequencies (e.g. Matsueda et al., 2009; Schiemann et al., 2020) and on improvements of storm-track biases in climate models (Schemm, 2023). We specifically make use of idealized aquaplanet climate model simulations with km-scale resolution and convection permitting limited to a region with an artificial SST front where, climatologically, diabatic heating associated with cyclogenesis occurs most frequently (Schemm, 2023). The SST-front mimics the zonal asymmetries imposed by the land-sea contrast and the Gulf Stream SST. Working with an aquaplanet enables us to better isolate the role that horizontal resolution has in favoring blocking events in the absence of other confounding factors (e.g. orography). We, therefore, investigate how such an idealized simulation can impact wintertime blocking frequencies downstream of a zonal asymmetry. We also address the generative mechanisms of the blocking events by conducting a Rossby-wave breaking analysis.

Section 2 describes the data and methods and, Section 3 shows our results in terms of blocking averages, difference maps of blocking frequencies, and wave-breaking analysis. Lastly, Section 4 contains the discussion and conclusions of our study.

2. Data and Methods

2.1 Model simulations

We use the idealized climate model simulations from Schemm (2023). These simulations were conducted with the ICOsahedral Non-hydrostatic weather and climate model (ICON) v2.6.4 (Zängl et al., 2015) in an aquaplanet setup. It includes parameterizations that follow the German Weather Service (DWD) operational standard configuration, such as a one-moment two-category microphysics scheme (Doms et al., 2011), non-orographic gravity wave drag (Orr et al., 2010), a prognostic TKE scheme for sub-gridscale turbulent transfer (Raschendorfer, 2001), and the radiation scheme ecRad (Hogan & Bozzo, 2018). The model has a global horizontal resolution of ~20 km (R2B7), a time step of 180 s and parameterized deep convection following Tiedtke (1989). A first regional nest with 10 km (R2B8) resolution employs a reduced scheme for shallow convection and in a second nest with, 5 km (R2B9) resolution, convection is not parameterized.

The two inner nests also interact bi-directionally and work with a smaller time step that is reduced by a factor of two, i.e., to 90 s and 45 s, respectively. They are located in the northern hemisphere (NH), and centered around the SST front, as illustrated in Figure S1. Both NH and southern hemisphere (SH) follow observed NH wintertime (DJF) zonal mean conditions and in both hemispheres an idealized SST anomaly is superimposed on the zonally symmetric background SST (termed "Qbos", see Neale & Hoskins (2000)), so that it can mimic the Gulf Stream and the land-sea contrasts over the coast of North America (Schemm, 2023). The simulations initially run for 10 perpetual years, with the solar zenith angle fixed over the equator at 90° as is common practice in aquaplanet studies. Besides the high-resolution nest, both hemispheres are symmetric. In order to quantify the influence of the km-scale resolution nest globally, the simulations are regridded to a common horizontal grid of 1°x1° and daily mean data are analyzed. Out of the original 10 perpetual winter years of simulations from Schemm (2023), we use a total of 1,315 days (i.e. 3.65 perpetual winter years or 14.6 winter seasons) which were the only ones available at the time of starting this study. For all our analyses, we use geopotential height at 500 hPa (Z500, m) and zonal U wind at 300 hPa (m s^{-1}). More details on the ICON simulations can be found in Schemm (2023).

2.2 Blocking and Rossby-wave breaking indices

We compute blocking by using geopotential at the 500 hPa level (Z500) and two algorithms denoted as the Anomaly (ANM, similar to Schwierz et al., 2004) and Absolute (ABS, similar to Davini et al., 2012) methods following Woollings et al. (2018). Both indices identify blocking occurrences, but they are based on different characteristics of the atmospheric flow, hence their results are not necessarily supposed to coincide (Scherrer et al., 2006; Woollings et al., 2018).

For computing blocking frequencies with the ANM method, we use the Contrack python package (Steinfeld et al., 2020). We compute daily Z500 anomalies at grid-point level as the daily mean departure from the daily mean climatology within the study period (no seasonality is present). Then, daily blocking events are computed as 2-D regions with Z500 anomalies larger than the 90^{th} percentiles of the daily Z500 anomaly distribution of all grid points between 50°-80°N, which

corresponds to 174 geopotential meters (gpm). We apply the same anomaly threshold to all grid points to detect instantaneous blocking. To guarantee quasi-stationarity and persistence we also impose a 50% minimum spatial overlap between the areas where instantaneous blocking occurs for each consecutive time step over a total period (lifetime) of at least 5 days. Note that the temporal granularity of our data is daily, compared to 6-hourly in many other studies, and hence we use a smaller overlap. We have tested the sensitivity to different values of overlap and anomaly threshold (see Supplementary Information) and found that the results are not very sensitive to the exact threshold chosen. However, the blocking frequency quickly decreases if a too-large overlap is chosen.

In the ABS method, areas are identified where the Z500 meridional gradient reverses. For computing blocking frequencies with the ABS method, we use the R package MiLES which is based on Davini et al. (2012) and additionally described in Davini (2018) and Woollings et al. (2018). The ABS method interpolates the data to 2.5°x2.5° horizontal resolution and checks, at each longitude, if Z500 decreases by at least 10m/° over a 15° segment north of the grid cell and, in addition, also decreases over a 15° segment to the south (see Eqs. A1-A3 in Davini et al. (2012)). Then, a grid point is defined as large-scale blocking if this condition is satisfied for at least a 15° continuous longitude and a blocking event occurs, if a large-scale blocking is observed within a 5° latitude × 10° longitude box centered on that grid point with a persistence of at least 5 days. In addition to this, Davini et al. (2012) also included additional criteria to determine if the reversal of the Z500 field is associated with anticyclonic (AC-) or cyclonic (C-) Rossby wave breaking (RWB). This distinction is made based on the zonal gradient of Z500 7.5° south of each blocked grid point, with respectively Z500 decreasing (for AC-RWB) and increasing (for C-RWB) over a 7.5° East/West segment centered at the blocking longitude. We note that the sum of AC-RWB and C-RWB events is not equivalent to the ABS blocking events, because we consider large-scale, temporally persistent blocking and not instantaneous blocking. For a complete derivation of the ABS and Rossby-wave breaking indices we refer the reader to Appendix A and D in Davini et al. (2012).

We also check the statistical significance of both blocking and Rossby wave frequencies by applying a two-sided z-test (Wilson, 1927) that compares two proportions, in our case being percentage of the events at grid-point level, one from the NH and the corresponding one from the SH. The z-test therefore tests the null hypothesis of whether the two proportions are statistically equal and by obtaining a p-value <0.05 one rejects the null hypothesis and considers the two proportions different with a 5% level of statistical significance.

3. Results

3.1 Blocking and Rossby-wave breaking average frequencies

Figure 1a-d shows the blocking frequencies (%), zonal wind averages (m s^{-1}) and the corresponding zonal mean daily blocking frequencies for both the ANM and ABS methods. For the ANM method, we observe a local maximum of ~11% of blocked days (out of 1315 days in total) in both the SH and NH downstream/east of the SST-front (0-100°E) (Figure 1a). The zonal average is above 6% blocking days around 65°N/S, i.e. poleward of the climatological position of the 500hPa jet (Figure 1b). The ABS method, on the other hand, shows an overall maximum frequency of ~7%, which is lower than for the ANM method, in both hemispheres (Figure 1c). This difference is expected because the two blocking indices are intrinsically different, while the ABS method identifies zones of geopotential reversal, the ANM method detects large and persistent geopotential anomalies, which are not necessarily always related to reversals of the mean flow. Moreover, we observe the peak number of blocking events at higher latitudes compared to the ANM method, near the poleward limits of the study area (i.e. 75°N and 75°S, Figure 1d). Lastly, there is a weak second maximum of ABS blocking over the subtropics (30°N and 30°S, Figure 1d). Such reversals of the Z500 gradient in the subtropics are associated with weaker Z500 anomalies (not captured by the ANM method) that typically are not even able to 'block' the zonal circulation in the midlatitudes. Zonal wind averages (m s^{-1}) show almost symmetrical patterns between the NH and SH, with very weak values at the poles (i.e. 0-13 m s^{-1}) that gradually increase toward the lower midlatitudes (i.e. at 30°N-40°N and 30°S-40°S), where they reach their maximum values of > 40 m s^{-1} from 50°W to 50°E (Figure 1a), east of the SST front (Schemm, 2023). As in observations, blocking and Rossby wave breaking, associated with a

reversal of the Z500 meridional gradient field as for the ABS blocking, tend to occur north of the climatological jet stream location, (Davini et al., 2012), which underpins the fact that essential blocking dynamics are captured by the idealized simulation. This pattern is also clearly shown in Figure 1e-h, which represent the averages of both anticyclonic (AC-RWB) and cyclonic (C-RWB) Rossby wave breaking events. When comparing our idealized blocking averages (Fig. 1a-d) with previous studies using reanalysis products (Davini et al., 2012; Woollings et al., 2018) we notice that our blocking frequencies are zonally more symmetric and the regional maxima are thus less pronounced compared to reanalysis, which is due to the zonally more symmetric aquaplanet setup that, e.g., does not feature land-sea contrasts. However, the meridional distributions of our blocking frequencies resemble the ones of the reanalyses.

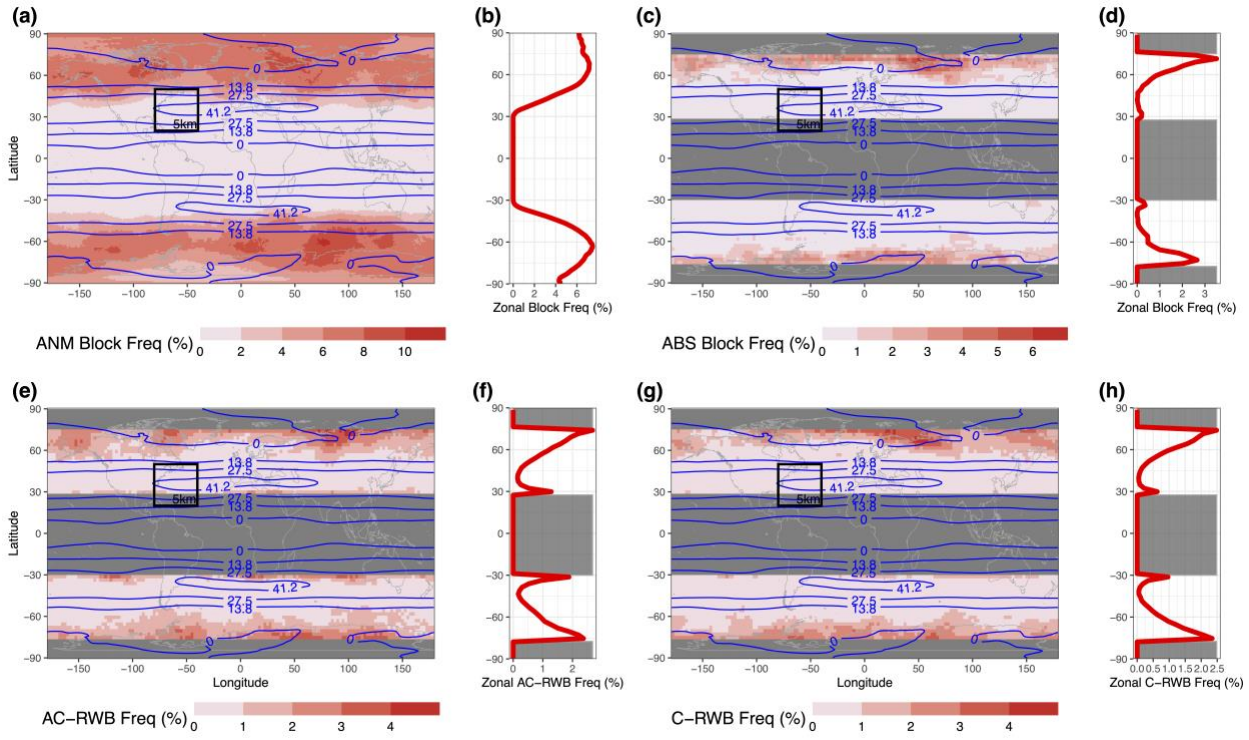

Figure 1. (a-d) Blocking and (e-h) Rossby-wave breaking average frequencies over the 14.6 boreal winter seasons of the ICON simulation. Blocking frequencies in (a-b) and (c-d) are computed with the Anomaly (ANM) and Absolute (ABS) method respectively. Rossby-wave breaking frequencies in (e-h) are computed following Davini et al. (2012). Anticyclonic and cyclonic wave breaking are shown in (e-f) and (g-h) respectively. In (b, d, f, h) the zonal frequencies of blocking and Rossby-wave breaking are presented. Blue contour lines represent the zonal U wind averages at 500 hPa (m s^{-1}) over the same time-period. Black

boxes indicate the 5 km convection permitting area of the idealized simulation. Continents are only drawn for illustrative purposes and are not present in the aquaplanet simulation.

3.2 Changes in blocking and Rossby wave-breaking frequencies

Figure 2 shows the blocking frequency difference between the NH, where the high-resolution, convection permitting nests are located, and the SH, with a uniform resolution of 20 km. Results for the ANM index point towards a significant (p-value <0.05) and widespread increase of blocking frequency over the Arctic region, between northern Canada and Svalbard (note that here land regions are only used as reference, as there is no representation of land in this aquaplanet simulation). Such an increase in blocking frequency over this region is consistent with what we would expect from a poleward shift and intensification of extratropical cyclones in the SST front area as observed in Schemm (2023) and Hermoso et al. (2024), and an upper-tropospheric outflow of low-PV air from the corresponding WCBs even further poleward . Another region showing an increase in blocking frequencies is central western North America and the northeastern Pacific, again associated with increased cyclone frequencies nearby to the south/southwest. On the other hand, the blocking frequency decreases over northeastern North America, eastern Europe and central Asia, which are regions where also the cyclone frequency tends to decrease, associated with the general poleward shift of the storm tracks. Similar results are obtained when changing the overlap area and the percentile threshold used in the blocking identification algorithm, although with lower thresholds (i.e. 80^{th} and 85^{th} percentiles), the signal over the Arctic gets weaker (Figure S2).

Differences for the ABS method show distinctive spatial patterns when compared to the ANM method, with a significant increase in blocking frequency over Eurasia (50°E-100°E, 60°N) and Alaska. The increase over Eurasia is located near the model's left-exit region of the jet streak originating from the SST front (see again Fig. 1). It is also located to the east of the enhanced northern hemispheric storm track's exit region, indicated by increased cyclone frequency (Schemm, 2023). More intense extratropical cyclones due to increased resolution in the SST front region may lead to enhanced wave breaking over that area at the end of their life cycle, which leads to more frequent reversal of the geopotential height gradient as measured by the ABS

method. The difference between both method is hence an expected result because both methods highlight different characteristics of blocking dynamics and Rossby wave breaking.

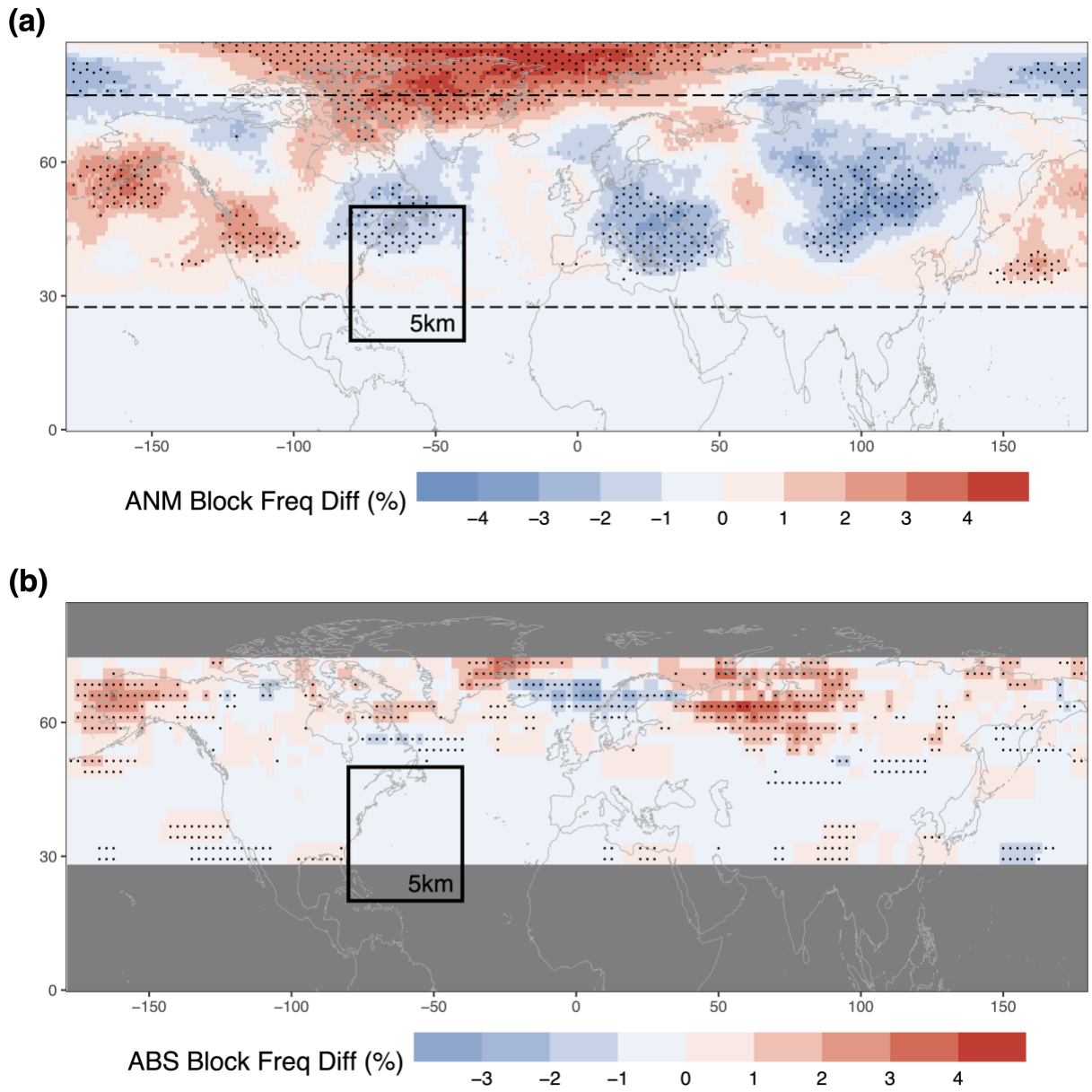

Figure 2. Difference between NH and SH for the (a) ANM and (b) ABS blocking frequencies (%). Stippling represents areas statistically significant at the 5% level (p-value <0.05) according to a proportion test. In (a) the two black horizontal dashed lines represent the geographical limits of (b) for comparison. Continents are only drawn for illustrative purposes and are not present in the aquaplanet simulation.

289 The enhanced ABS blocking frequency can be further decomposed into contributions from
290 anticyclonic and cyclonic wave breaking associated with a reversal of the Z500 meridional
291 gradient field (Davini et al., 2012), as shown in Fig. 3. While the increase over Alaska is almost
292 entirely due to an increase in anticyclonic wave breaking, the signal over Russia is related to both
293 enhanced cyclonic wave breaking in its western part and enhanced anticyclonic wave breaking
294 further east. This west-east dipole of cyclonic and anticyclonic wave breaking represents an
295 increase or extension of the wave breaking location, as the positive anomalies are larger than the
296 negative ones. This is expected from the strengthening and tilting of the storm track in the very-
297 high resolution hemisphere, as shown in Schemm (2023). The fact that wave breaking anomalies
298 occur in a west-east dipole provides evidence of the realistic representation of these dynamical
299 processes in our idealized model, since such a dipole is also present in the wave-breaking
300 climatology over the North Atlantic based on reanalysis data (Tamarin-Brodsky & Harnik, 2024).
301 We also computed Rossby-wave breaking difference maps following the methodology proposed
302 by Barnes & Hartmann (2012) and using Z500 instead of PV (Text S1 and Figure S3). This
303 alternative index shows consistent results, with a significant increase in anticyclonic and cyclonic
304 wave breaking in the same range of longitudes as the Davini et al. (2012) method.
305

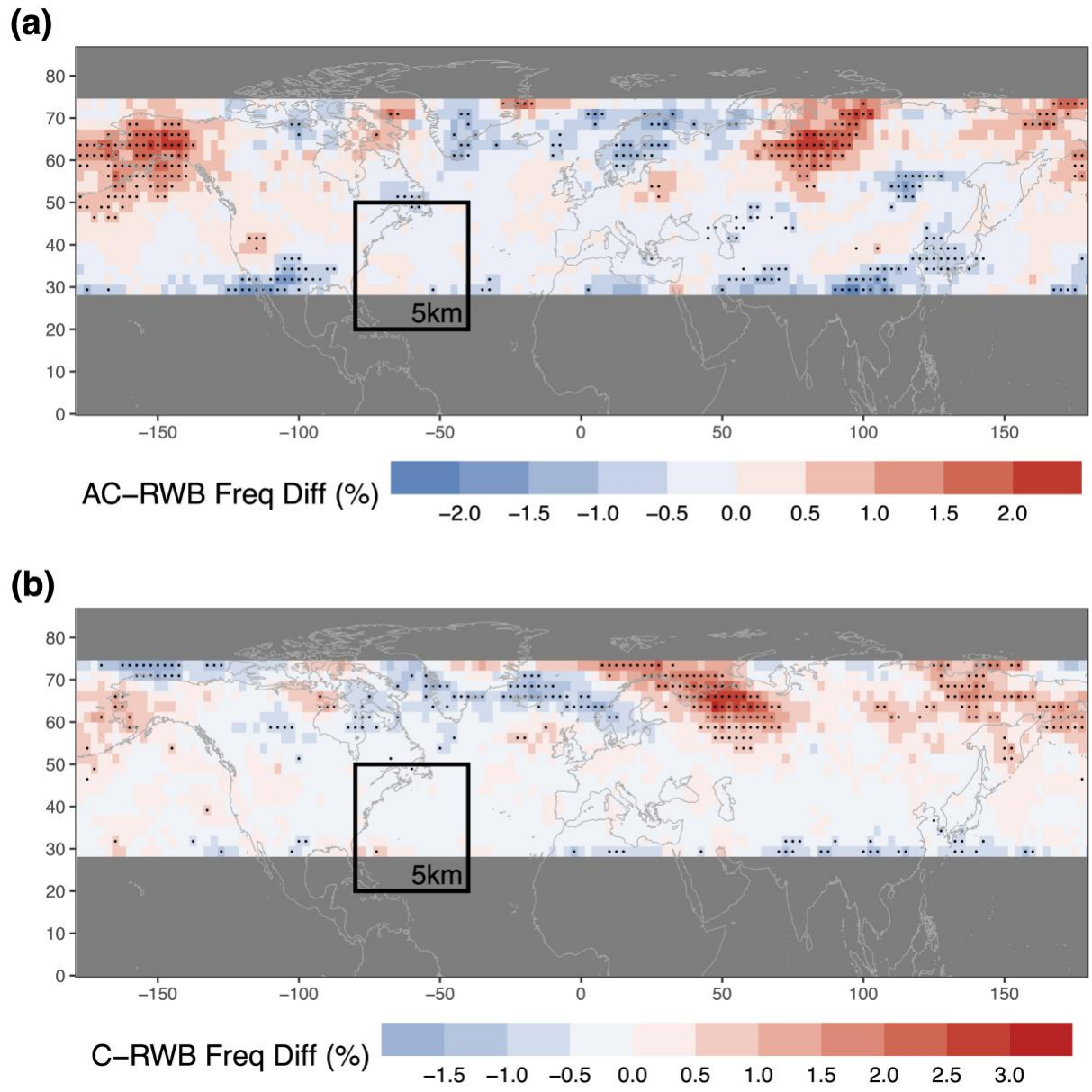

Figure 3. Difference maps of Rossby-wave breaking frequencies computed from a reversal of the Z500 meridional gradient field. (a) Anticyclonic and (b) cyclonic wave-breaking events computed following Davini et al. (2012). Stippling represent areas statistically significant at the 5% level (p-value <0.05) according to a proportion test. Continents are only drawn for illustrative purposes and are not present in the aquaplanet simulation.

4. Discussion and Conclusions

In this work, we have used an idealized very-high resolution convection permitting simulation with the ICON climate model in aquaplanet setup (Schemm, 2023) to quantify the impact of such

316 a high resolution on blocking and Rossby-wave breaking frequencies. We analyze a total of 14.6
317 boreal winter seasons, symmetrically in the SH (low) and NH (high resolution). To quantify the
318 impact of resolution on cyclone-related diabatic processes, the NH has been simulated with two
319 bi-directionally interacting nested grids of 10 and 5 km grid spacing centered around an idealized
320 SST front. The highest-resolution nested domain allows for convective processes to occur without
321 being parameterized. Our results indicate that increased resolution in the region of extratropical
322 cyclone growth leads to increased blocking frequencies. The exact region of enhanced blocking
323 occurrence depends on the blocking index. An index identifying stationary anticyclones indicates
324 more frequent blocking poleward of the region where also the cyclone frequency increases due
325 to a more explicit representation of diabatic processes with high resolution (Schemm, 2023). This
326 is consistent with the hypothesis that diabatic processes amplify cyclones and the associated
327 WCBs, leading to enhanced poleward outflow of low-PV air masses in the middle and upper
328 troposphere that reinforce stationary anticyclones (Pfahl et al., 2015; Steinfeld et al., 2020;
329 Steinfeld & Pfahl, 2019). On the contrary, an index associating blocking with a reversal of
330 meridional geopotential height contours and thus wave breaking rather indicates more frequent
331 blocking further downstream, east of the strengthened storm track, where the more frequent
332 cyclones are associated with enhanced cyclonic and anti-cyclonic wave breaking at the end of
333 their life cycle (Figure S4).
334
335 Previous studies (e.g. Athanasiadis et al., 2022; Matsueda et al., 2009; Scaife et al., 2011;
336 Schiemann et al., 2020) have already shown that increasing spatial resolution can be beneficial
337 for the representation of blocking in climate models. Due to the importance of diabatic
338 processes, going to even higher, convection permitting resolution is hypothesized to further
339 reduce blocking biases, but this has not been explicitly tested so far due to the lack of global
340 climate simulations with such high-resolution spanning sufficiently long periods. Here we have
341 corroborated this hypothesis based on an idealized aquaplanet setup. This may have important
342 implications also for the next generation of convection permitting global climate models. Current
343 climate models still underestimate blocking frequencies. In particular, they underestimate the
344 occurrence of stationary anticyclones (ANM blocking) over the North Atlantic and the occurrence

of wave breaking (ABS blocking) further downstream over Eurasia (Woollings et al., 2018). Our results indicate that a higher resolution and better representation of diabatic processes over the SST front may increase ANM blocking closer to this SST front region and ABS blocking further downstream, thus potentially reducing both of these biases. This makes us optimistic that blocking biases will be reduced in convection permitting global climate simulations, eventually leading to more reliable estimates of changes of this important weather pattern in a warming climate.

Acknowledgments

PDL has received funding from the European Union's Horizon Europe Research and Innovation Programme under Grant Agreement No. 101059659.

Open Research

Data – The ICON simulation data, blocking and Rossby-wave breaking indices used in the study can be obtained from De Luca et al. (2024). Software – The softwares used for computing the blocking and Rossby-wave breaking indices are freely available from: i) Steinfeld (2020); ii) Davini (2018); and iii) Kaderli (2023).

References

Athanasiadis, P. J., Ogawa, F., Omrani, N.-E., Keenlyside, N., Schiemann, R., Baker, A. J., et al. (2022). Mitigating Climate Biases in the Midlatitude North Atlantic by Increasing Model Resolution: SST Gradients and Their Relation to Blocking and the Jet. *Journal of Climate*, *35*(21), 6985–7006. https://doi.org/https://doi.org/10.1175/JCLI-D-21-0515.1

Barnes, E. A., & Hartmann, D. L. (2012). Detection of Rossby wave breaking and its response to shifts of the midlatitude jet with climate change. *Journal of Geophysical Research: Atmospheres*, *117*(D9). https://doi.org/https://doi.org/10.1029/2012JD017469

Cai, W., Xu, X., Cheng, X., Wei, F., Qiu, X., & Zhu, W. (2020). Impact of “blocking” structure in the troposphere on the wintertime persistent heavy air pollution in northern China. *Science of The Total Environment*, *741*, 140325.

https://doi.org/https://doi.org/10.1016/j.scitotenv.2020.140325

Davini, P. (2018). MiLES - Mid Latitude Evaluation System [Software]. *Zenodo*. Retrieved from http://doi.org/10.5281/zenodo.1237837

Davini, P., & D'Andrea, F. (2020). From CMIP3 to CMIP6: Northern Hemisphere Atmospheric Blocking Simulation in Present and Future Climate. *Journal of Climate*, *33*(23), 10021–10038. https://doi.org/https://doi.org/10.1175/JCLI-D-19-0862.1

Davini, P., Cagnazzo, C., Gualdi, S., & Navarra, A. (2012). Bidimensional Diagnostics, Variability, and Trends of Northern Hemisphere Blocking. *Journal of Climate*, *25*(19), 6496–6509. https://doi.org/https://doi.org/10.1175/JCLI-D-12-00032.1

Doms, G., Förstner, J., Heise, E., Herzog, H.-J., Mironov, D., Raschendorfer, M., et al. (2011). *A description of the nonhydrostatic regional COSMO model Part II: Physical parameterization*.

Eyring, V., Bony, S., Meehl, G. A., Senior, C. A., Stevens, B., Stouffer, R. J., & Taylor, K. E. (2016). Overview of the Coupled Model Intercomparison Project Phase 6 (CMIP6) experimental design and organization. *Geosci. Model Dev.*, *9*(5), 1937–1958. https://doi.org/10.5194/gmd-9-1937-2016

Haarsma, R. J., Roberts, M. J., Vidale, P. L., Senior, C. A., Bellucci, A., Bao, Q., et al. (2016). High Resolution Model Intercomparison Project (HighResMIP~v1.0) for CMIP6. *Geoscientific Model Development*, *9*(11), 4185–4208. https://doi.org/10.5194/gmd-9-4185-2016

Hermoso, A., Rivière, G., Harvey, B., Methven, J., & Schemm, S. (2024). A dynamical interpretation of the intensification of the winter North Atlantic jet stream in reanalysis. *Journal of Climate*. https://doi.org/https://doi.org/10.1175/JCLI-D-23-0757.1

Hogan, R. J., & Bozzo, A. (2018). A Flexible and Efficient Radiation Scheme for the ECMWF Model. *Journal of Advances in Modeling Earth Systems*, *10*(8), 1990–2008. https://doi.org/https://doi.org/10.1029/2018MS001364

Kaderli, S. (2023). WaveBreaking - Detection, Classification and Tracking of Rossby Wave Breaking [Software]. *Zenodo*. Retrieved from https://doi.org/10.5281/zenodo.8123188

Kautz, L.-A., Martius, O., Pfahl, S., Pinto, J. G., Ramos, A. M., Sousa, P. M., & Woollings, T. (2022). Atmospheric blocking and weather extremes over the Euro-Atlantic sector -- a review. *Weather and Climate Dynamics*, *3*(1), 305–336. https://doi.org/10.5194/wcd-3-

305-2022

De Luca, P., Jiménez-Esteve, B., Degenhardt, L., Schemm, S., & Pfahl, S. (2024). Datasets used in "Enhanced Blocking Frequencies in Very-high Resolution Idealized Climate Model Simulations" [Data]. *Zenodo*. https://doi.org/10.5281/zenodo.12575399

Lupo, A. R. (2021). Atmospheric blocking events: a review. *Annals of the New York Academy of Sciences*, *1504*(1), 5–24. https://doi.org/https://doi.org/10.1111/nyas.14557

Madonna, E., Wernli, H., Joos, H., & Martius, O. (2014). Warm Conveyor Belts in the ERA-Interim Dataset (1979–2010). Part I: Climatology and Potential Vorticity Evolution. *Journal of Climate*, *27*(1), 3–26. https://doi.org/https://doi.org/10.1175/JCLI-D-12-00720.1

Matsueda, M. (2011). Predictability of Euro-Russian blocking in summer of 2010. *Geophysical Research Letters*, *38*(6). https://doi.org/https://doi.org/10.1029/2010GL046557

Matsueda, M., Mizuta, R., & Kusunoki, S. (2009). Future change in wintertime atmospheric blocking simulated using a 20-km-mesh atmospheric global circulation model. *Journal of Geophysical Research: Atmospheres*, *114*(D12). https://doi.org/https://doi.org/10.1029/2009JD011919

Matsueda, M., Endo, H., & Mizuta, R. (2010). Future change in Southern Hemisphere summertime and wintertime atmospheric blockings simulated using a 20-km-mesh AGCM. *Geophysical Research Letters*, *37*(2). https://doi.org/https://doi.org/10.1029/2009GL041758

Nakamura, N., & Huang, C. S. Y. (2018). Atmospheric blocking as a traffic jam in the jet stream. *Science*, *361*(6397), 42–47. https://doi.org/10.1126/science.aat0721

Narinesingh, V., Booth, J. F., Clark, S. K., & Ming, Y. (2020). Atmospheric blocking in an aquaplanet and the impact of orography. *Weather and Climate Dynamics*, *1*(2), 293–311. https://doi.org/10.5194/wcd-1-293-2020

Neale, R. B., & Hoskins, B. J. (2000). A standard test for AGCMs including their physical parametrizations: I: the proposal. *Atmospheric Science Letters*, *1*(2), 101–107. https://doi.org/https://doi.org/10.1006/asle.2000.0022

Orr, A., Bechtold, P., Scinocca, J., Ern, M., & Janiskova, M. (2010). Improved Middle Atmosphere Climate and Forecasts in the ECMWF Model through a Nonorographic Gravity Wave Drag

Parameterization. *Journal of Climate*, *23*(22), 5905–5926. https://doi.org/https://doi.org/10.1175/2010JCLI3490.1

Pfahl, S., & Wernli, H. (2012). Quantifying the relevance of atmospheric blocking for co-located temperature extremes in the Northern Hemisphere on (sub-)daily time scales. *Geophysical Research Letters*, *39*(12). https://doi.org/https://doi.org/10.1029/2012GL052261

Pfahl, S., Schwierz, C., Croci-Maspoli, M., Grams, C. M., & Wernli, H. (2015). Importance of latent heat release in ascending air streams for atmospheric blocking. *Nature Geoscience*, *8*(8), 610–614.

Pithan, F., Shepherd, T. G., Zappa, G., & Sandu, I. (2016). Climate model biases in jet streams, blocking and storm tracks resulting from missing orographic drag. *Geophysical Research Letters*, *43*(13), 7231–7240. https://doi.org/https://doi.org/10.1002/2016GL069551

Raschendorfer, M. (2001). *The new turbulence parameterization of LM*.

Scaife, A. A., Woollings, T., Knight, J., Martin, G., & Hinton, T. (2010). Atmospheric Blocking and Mean Biases in Climate Models. *Journal of Climate*, *23*(23), 6143–6152. https://doi.org/https://doi.org/10.1175/2010JCLI3728.1

Scaife, A. A., Copsey, D., Gordon, C., Harris, C., Hinton, T., Keeley, S., et al. (2011). Improved Atlantic winter blocking in a climate model. *Geophysical Research Letters*, *38*(23). https://doi.org/https://doi.org/10.1029/2011GL049573

Schemm, S. (2023). Toward Eliminating the Decades-Old "Too Zonal and Too Equatorward" Storm-Track Bias in Climate Models. *Journal of Advances in Modeling Earth Systems*, *15*(2), e2022MS003482. https://doi.org/https://doi.org/10.1029/2022MS003482

Scherrer, S. C., Croci-Maspoli, M., Schwierz, C., & Appenzeller, C. (2006). Two-dimensional indices of atmospheric blocking and their statistical relationship with winter climate patterns in the Euro-Atlantic region. *International Journal of Climatology*, *26*(2), 233–249. https://doi.org/https://doi.org/10.1002/joc.1250

Schiemann, R., Athanasiadis, P., Barriopedro, D., Doblas-Reyes, F., Lohmann, K., Roberts, M. J., et al. (2020). Northern Hemisphere blocking simulation in current climate models: evaluating progress from the Climate Model Intercomparison Project Phase˜5 to 6 and sensitivity to resolution. *Weather and Climate Dynamics*, *1*(1), 277–292.

https://doi.org/10.5194/wcd-1-277-2020

Schwierz, C., Croci-Maspoli, M., & Davies, H. C. (2004). Perspicacious indicators of atmospheric blocking. *Geophysical Research Letters*, *31*(6). https://doi.org/https://doi.org/10.1029/2003GL019341

Steinfeld, D. (2020). ConTrack - Contour Tracking [Software]. *GitHub*. Retrieved from https://github.com/steidani/ConTrack

Steinfeld, D., & Pfahl, S. (2019). The role of latent heating in atmospheric blocking dynamics: a global climatology. *Climate Dynamics*, *53*(9), 6159–6180. https://doi.org/10.1007/s00382-019-04919-6

Steinfeld, D., Boettcher, M., Forbes, R., & Pfahl, S. (2020). The sensitivity of atmospheric blocking to upstream latent heating -- numerical experiments. *Weather and Climate Dynamics*, *1*(2), 405–426. https://doi.org/10.5194/wcd-1-405-2020

Tamarin-Brodsky, T., & Harnik, N. (2024). The relation between Rossby wave-breaking events and low-level weather systems. *Weather and Climate Dynamics*, *5*(1), 87–108. https://doi.org/10.5194/wcd-5-87-2024

Taylor, K. E., Stouffer, R. J., & Meehl, G. A. (2012). An Overview of CMIP5 and the Experiment Design. *Bulletin of the American Meteorological Society*, *93*(4), 485–498. https://doi.org/https://doi.org/10.1175/BAMS-D-11-00094.1

Tiedtke, M. (1989). A Comprehensive Mass Flux Scheme for Cumulus Parameterization in Large-Scale Models. *Monthly Weather Review*, *117*(8), 1779–1800. https://doi.org/https://doi.org/10.1175/1520-0493(1989)117<1779:ACMFSF>2.0.CO;2

Wilson, E. B. (1927). Probable Inference, the Law of Succession, and Statistical Inference. *Journal of the American Statistical Association*, *22*(158), 209–212. https://doi.org/10.1080/01621459.1927.10502953

Woollings, T., Barriopedro, D., Methven, J., Son, S.-W., Martius, O., Harvey, B., et al. (2018). Blocking and its Response to Climate Change. *Current Climate Change Reports*. https://doi.org/10.1007/s40641-018-0108-z

Yamamoto, A., Nonaka, M., Martineau, P., Yamazaki, A., Kwon, Y.-O., Nakamura, H., & Taguchi, B. (2021). Oceanic moisture sources contributing to wintertime Euro-Atlantic blocking.

Weather and Climate Dynamics, *2*(3), 819–840. https://doi.org/10.5194/wcd-2-819-2021

Yamazaki, A., & Itoh, H. (2013). Vortex–Vortex Interactions for the Maintenance of Blocking. Part I: The Selective Absorption Mechanism and a Case Study. *Journal of the Atmospheric Sciences*, *70*(3), 725–742. https://doi.org/https://doi.org/10.1175/JAS-D-11-0295.1

Zängl, G., Reinert, D., Rípodas, P., & Baldauf, M. (2015). The ICON (ICOsahedral Non-hydrostatic) modelling framework of DWD and MPI-M: Description of the non-hydrostatic dynamical core. *Quarterly Journal of the Royal Meteorological Society*, *141*(687), 563–579. https://doi.org/https://doi.org/10.1002/qj.2378

519 Supporting Information for

520 Enhanced Blocking Frequencies in Very-high Resolution Idealized Climate Model 521 Simulations

522 P. De Luca[1,2], B. Jiménez-Esteve[3], L. Degenhardt[2], S. Schemm[4], and S. Pfahl[2]

523 1. Barcelona Supercomputing Center (BSC), Barcelona, Spain

524 2. Institute of Meteorology - Freie Universität Berlin, Berlin, Germany

525 3. Instituto de Geociencias (IGEO), Consejo Superior de Investigaciones Científicas–Universidad Complutense de
526 Madrid (CSIC–UCM), Madrid, Spain

527 4. Institute for Atmospheric and Climate Science - ETH Zürich, Zürich, Switzerland

528

529 **Contents of this file**

530

531 Text S1
532 Figures S1 to S4

533

534 **Introduction**

535 This Supporting Information provides extra details on a second method used for computing Rossby-wave
536 breaking along with three supporting figures that describe the nested areas used in the idealized climate
537 model simulations, difference maps of ANM blocking frequencies computed with other overlapping areas
538 and percentiles than in the main text, and difference maps of Rossby-wave breaking computed with the
539 second method here described.

540

541

542 **Text S1.**

543 For computing anticyclonic and cyclonic wave-breaking frequencies we also use a second algorithm
544 introduced by Barnes & Hartmann (2012). This algorithm searches for synoptic-scale wave-breaking of a
545 given field by quantifying regions where the contours overturn using potential vorticity (PV) contours
546 (usually 2PVU is taken). In our case, as we do not have PV available, we have substituted PV for Z500 and
547 tested results using different contours but found that the 5300 gpm contour gives the most sensible result.
548 To quantify wave-breaking events, the longest closed contour encircling the field's pole is identified. Then,
549 the algorithm searches the locations where a single meridian intersects the contour at least three times. Such
550 locations are named overturning points, and if they occur within 500 km of each other and within the same
551 contour, they are considered part of the same event. Then, the algorithm groups the overturning contours
552 into daily wave-breaking events by quantifying contiguous contours that all have overturning centers (i.e.
553 geographic centers of the overturning points) within 2000 km of each other. If this condition is not fulfilled,
554 different wave-breaking events are created. The center of a wave-breaking event is defined as the
555 geographic center of all grid points on all contours in the event (Barnes & Hartmann, 2012).

556

557 The detection algorithm also differentiates between cyclonic and anticyclonic wave-breaking events, or
558 breaking events that overturn cyclonically and anticyclonically. In our case, when we use Z500 instead of

PV, this is done by ordering the overturning points from west to east, so that in the Northern hemisphere cyclonic events are quantified as those whose west-most overturning point is equatorward of the east-most overturning point and anticyclonic ones as those whose west-most overturning point is poleward of the east-most overturning point. In the Southern Hemisphere the definition is the opposite. To consider the possibility that one wave-breaking event lasts more than one day the algorithm also groups the events in time that have a center within 2000 km of each other (Barnes & Hartmann, 2012). Here, we compute cyclonic and anticyclonic Rossy wave-breaking by using daily Z500 fields at 1°x1° horizontal resolution from the ICON simulation of Schemm (2023) and using the python library WaveBreaking v0.3.7 (Kaderli, 2023).

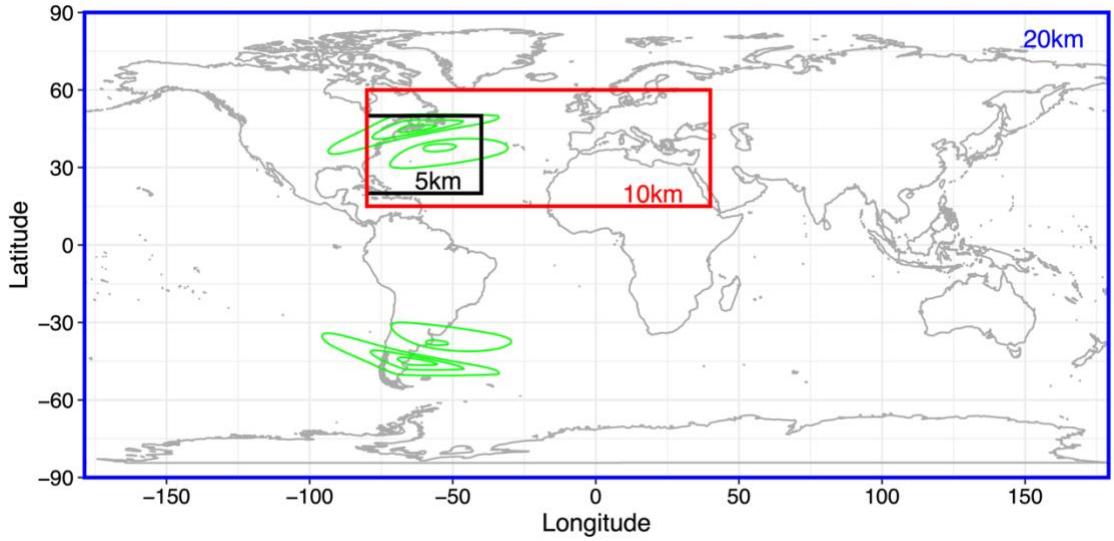

Figure S1. Horizontal resolution (km) of the nested areas used in the ICON simulations. Black: 5 km; red: 10 km; and blue: 20 km. These correspond to the same resolution and areas of Schemm (2023). Green contours show the idealized sea-surface temperature front computed from 2m temperatures after removing the zonal mean. Continents are only drawn for illustrative purposes and are not present in the aquaplanet simulation.

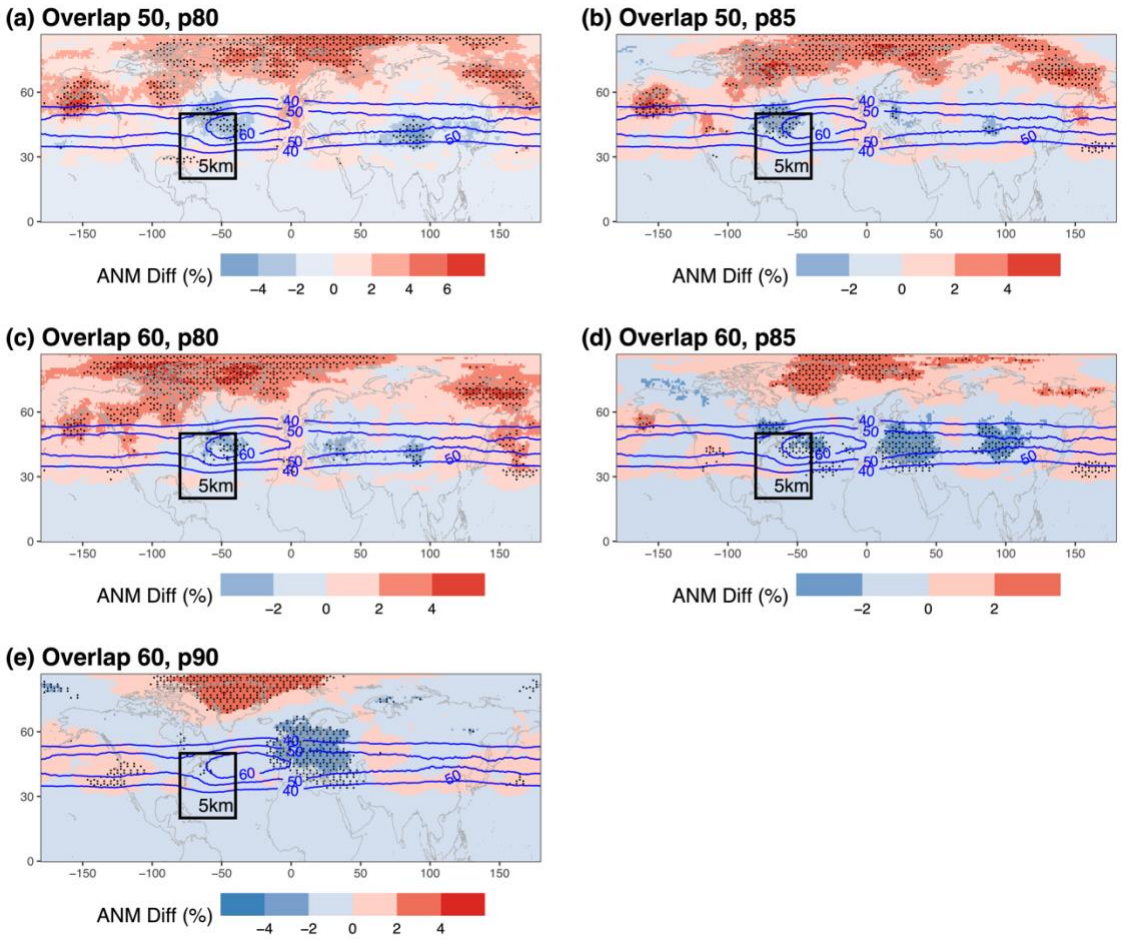

Figure S2. As Figure 2a but for ANM blocking frequency differences (%) computed with (a) overlap 50 and 80th percentile, (b) 50 and 85th, (c) 60 and 80th, (d) 60 and 85th and (e) 60 and 90th. Continents are only drawn for illustrative purposes and are not present in the aquaplanet simulation.

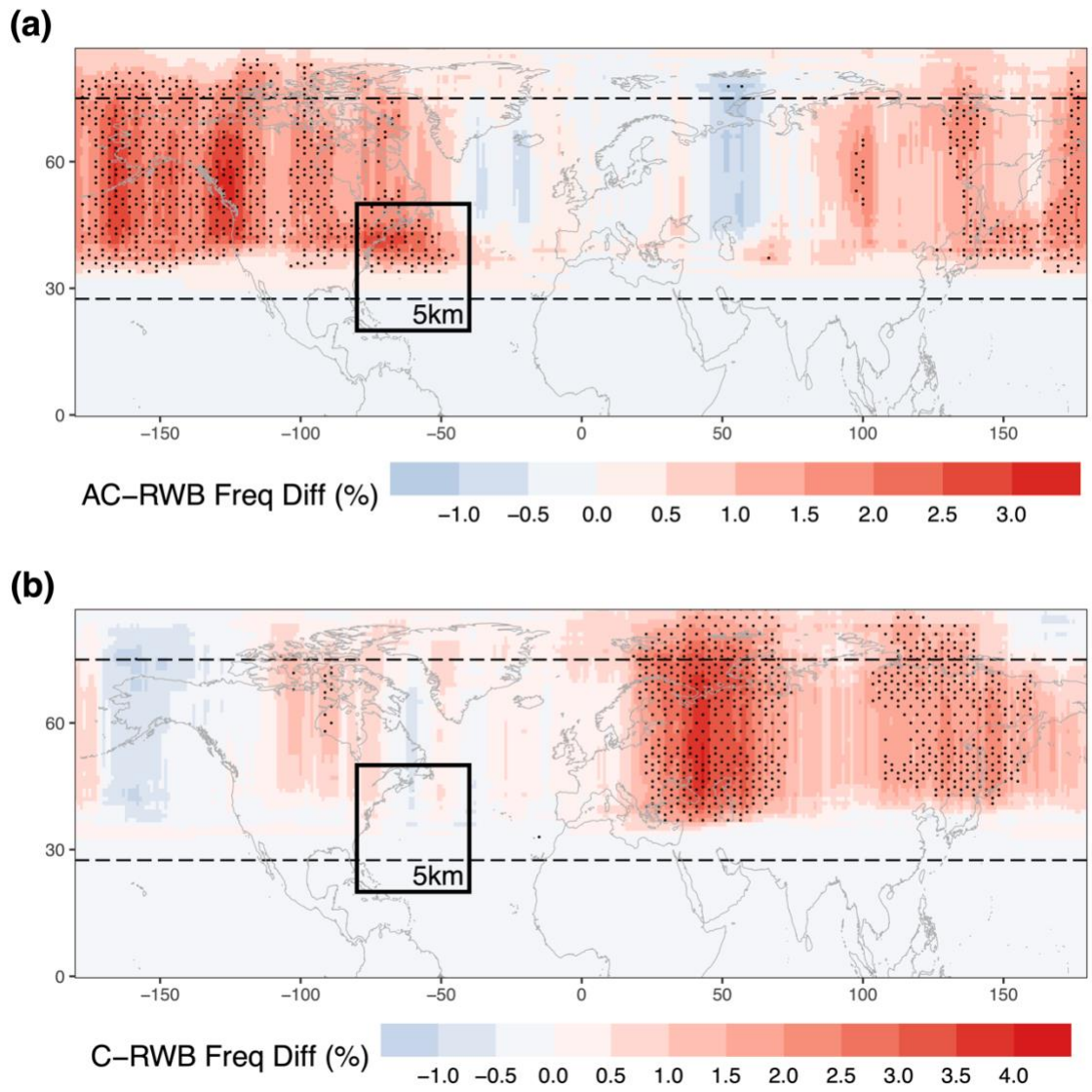

Figure S3. Same as Figure 3 but with Rossby-wave breaking computed following Barnes & Hartmann (2012). Black horizontal lines represent the geographical limits of the Davini et al. (2012) RWB method for comparison. Continents are only drawn for illustrative purposes and are not present in the aquaplanet simulation.

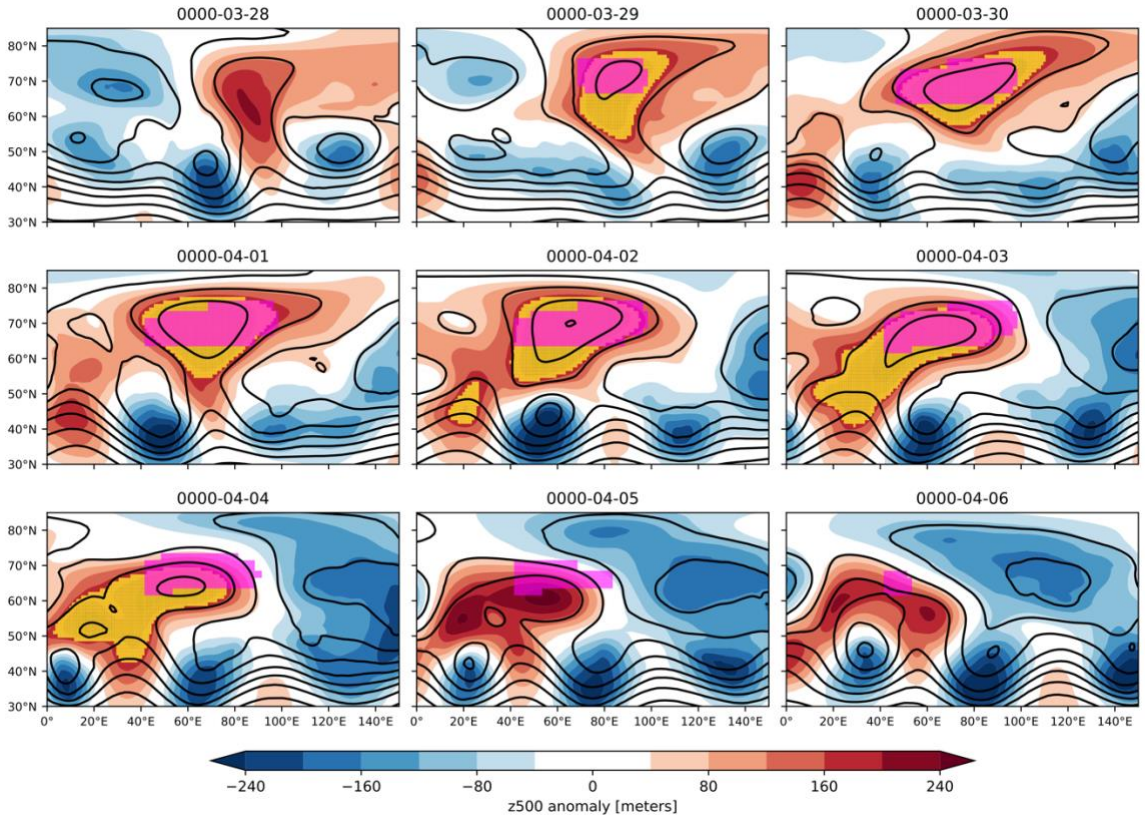

Figure S4. Case-study of a blocking event using geopotential height (m) anomalies at 500hPa (z500). Each panel represent a single day. Yellow and pink grid-points show respectively the ANM and ABS blocking indices.

References

Barnes, E. A., & Hartmann, D. L. (2012). Detection of Rossby wave breaking and its response to shifts of the midlatitude jet with climate change. *Journal of Geophysical Research: Atmospheres*, *117*(D9). https://doi.org/https://doi.org/10.1029/2012JD017469

Davini, P., Cagnazzo, C., Gualdi, S., & Navarra, A. (2012). Bidimensional Diagnostics, Variability, and Trends of Northern Hemisphere Blocking. *Journal of Climate*, *25*(19), 6496–6509. https://doi.org/https://doi.org/10.1175/JCLI-D-12-00032.1

Kaderli, S. (2023). WaveBreaking - Detection, Classification and Tracking of Rossby Wave Breaking [Software]. *Zenodo*. Retrieved from https://doi.org/10.5281/zenodo.8123188

Schemm, S. (2023). Toward Eliminating the Decades-Old "Too Zonal and Too Equatorward" Storm-Track Bias in Climate Models. *Journal of Advances in Modeling Earth Systems*, *15*(2), e2022MS003482. https://doi.org/https://doi.org/10.1029/2022MS003482